

Stable Implementation of a Deterministic Multi-Subband Boltzmann Solver for Silicon Double-Gate nMOSFETs

Kai Zhao^{*†}, Sung-Min Hong^{*}, Christoph Jungemann^{*}, and Ru-Qi Han[†]

^{*}EIT4, Bundeswehr University, 85577 Neubiberg, Germany

Email: k.zhao.chn@gmail.com

[†]Institute of Microelectronics, Peking University, 100871 Beijing, China

Abstract— Silicon Double Gate nMOSFETs are simulated using a deterministic Boltzmann solver coupled with a 1D Schrödinger and 2D Poisson Equation. Subthreshold characteristics and high drain bias conditions can be well simulated by the solver stabilized by the H-transformation and the maximum entropy dissipation scheme.

I. INTRODUCTION

Multisubband device simulations based on the Boltzmann Transport Equation (BTE) have been widely used to calculate Current-Voltage characteristics of MOSFETs [1]–[3]; however, for certain bias conditions, e.g. subthreshold difficulties are encountered due to either numerical issues of the deterministic solvers [3] or inefficiency of the Monte-Carlo solvers [4]. In this paper, a robust BTE solver based on Fourier expansion of arbitrary order is demonstrated. With this solver it is even possible to obtain stable solutions in subthreshold with high numerical accuracy and acceptable CPU times.

II. METHODOLOGY

The 2D device is partitioned into many slices along the transport direction (y -direction), and the subband structure is calculated by a 1D Schrödinger Equation (SE) for each slice, where x is the quantization direction. The electrostatic potential is calculated by the 2D Poisson Equation (PE) for the whole device. Four elliptical and two spherical valleys with parabolic band structures are used, and currently only phonon and surface roughness scattering are considered, where the models are similar to the ones used by Lucci et al. [2]. The acoustic deformation potential is chosen to be 12.9eV [5], and bulk values are kept for other phonon scattering parameters. The electron distribution function is projected onto equienergy surfaces in the 2D k -space, and then expanded into Fourier harmonics with respect to the angle:

$$f^{i,\nu}(y, \varepsilon, \phi) = \sum_{m=0}^M f_m^{i,\nu}(y, \varepsilon) Y_m(\phi) \quad (1)$$

where i, ν are the index of subband and valley, respectively,

and Y_m is defined as [3].

$$Y_m(\phi) = \sqrt{\frac{1}{(1 + \delta_{m,0}) \pi}} \cos(m\phi + \varphi_m),$$

$$\text{with } -M \leq m \leq M, \varphi_m = \begin{cases} 0 & m \geq 0 \\ \frac{\pi}{2} & m < 0 \end{cases} \quad (2)$$

Self-consistency among the SE, PE, and BTE is established by a Gummel-type relaxation scheme, and convergence is judged by the maximum change of the electrostatic potential after each iteration. During each SE, PE and BTE iteration, a Newton loop is adopted to insure the convergence of the BTE, which is non-linear due to the Pauli principle. The initial guess of the distribution function is given by a Fermi-Dirac distribution, whose quasi-Fermi level is calculated by a DD model according to the applied bias. The convergence of the Newton iteration is judged by the norm of the residue.

The box integration method, which insures conservation of densities and fluxes, is used based on a dual mesh in the real space. The discretization of the energy space is critical for the stabilization of the solver. Therefore, the H-transformation [6] is adopted by introducing the new coordinate (y, H) to replace $(y, \varepsilon_{\parallel})$, where $H = \varepsilon_{\parallel} + \varepsilon_{\perp}$ is the total energy, ε_{\parallel} the kinetic energy, and ε_{\perp} the minimum subband energy calculated by the SE. The energy space will be re-meshed every time after solving the SE because of the change of minimum subband energy. After the H-transformation, the free streaming operator only contains a differential operator with respect to position and is formulated in such a way that it satisfies the maximum entropy dissipation scheme [7], [8], and it reads:

$$\frac{1}{(2\pi)^2} \int \{LHS\} \delta \left(\varepsilon_{\parallel} - \varepsilon_{\parallel}^{i,\nu} (y, \vec{k}) \right) Y_m(\phi) dk^2$$

$$= \hat{T} \sum_{m'=0}^M \left[a_{m,m'} Z^{i,\nu} \frac{\partial v^{i,\nu}(y, H^{i,\nu}) f_m^{i,\nu}(y, H^{i,\nu})}{\partial y} \right.$$

$$\left. - \frac{F^{i,\nu}(y) Z^{i,\nu}}{\hbar k^{*,i,\nu}(y, H^{i,\nu})} b_{m,m'} f_m^{i,\nu}(y, H^{i,\nu}) \right] \quad (3)$$

where \hat{T} is the Herring-Vogt transformation coefficient, $Z^{i,\nu}$ the density of state, $v^{i,\nu}$ the electron velocity, $F^{i,\nu}$ the force and $a_{m,m'}$ and $b_{m,m'}$ the triple product of Fourier Harmonics,

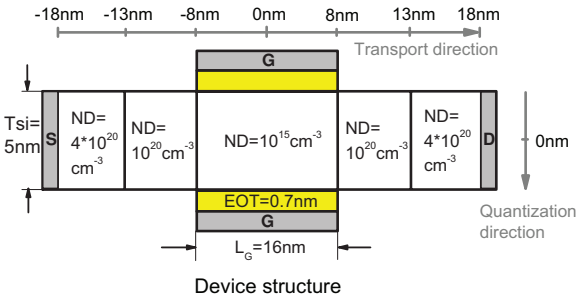


Fig. 1. Silicon double gate nMOSFET structure and doping profile

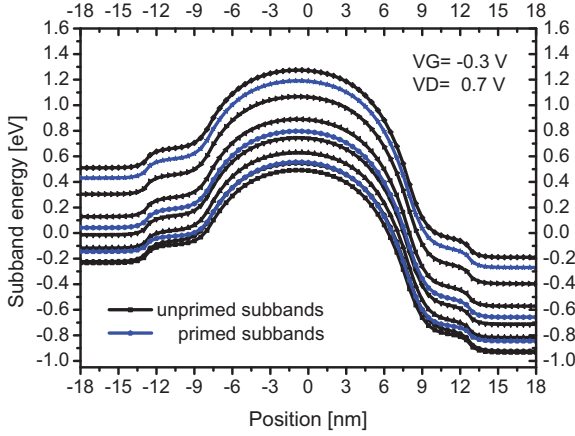


Fig. 2. Minimum subband energies in the H-space at $V_G=-0.1\text{V}$ and $V_D=0.7\text{V}$

which are defined as:

$$a_{m,m'} = \sqrt{\pi} \int_0^{2\pi} Y_m(\phi) Y_{m'}(\phi) Y_1(\phi) d\phi \quad (4)$$

$$b_{m,m'} = m \sqrt{\pi} \int_0^{2\pi} Y_{-m}(\phi) Y_{m'}(\phi) Y_{-1}(\phi) d\phi$$

III. RESULTS

Simulation results are presented for a silicon double gate nMOSFET with 16nm gate length (Fig. 1). The EOT of the gate oxides is 0.7nm, and the Si body thickness 5nm. A lattice temperature of 300K is assumed for all calculations. In y -direction a grid spacing of 0.5nm and in x of 0.1nm is used (73×65 grid nodes). The energy spacing is 5meV for the H-mesh ranging at most from -0.8eV to 1.4eV depending on the bias conditions (Fig. 2) and resulting in a maximum of about 2800000 unknowns for the BTE expanded with 8 Fourier harmonics. Filling the Jacobian matrix and solving the BTE consumes the largest part of the CPU time, where the total CPU time for one bias point is 5h or less on a single CPU core and the memory requirement a few GBytes.

The convergence of the electrostatic potential in the Gummel-type relaxation loop is shown in Fig. 3. As expected, convergence requires more iterations for a higher drain bias

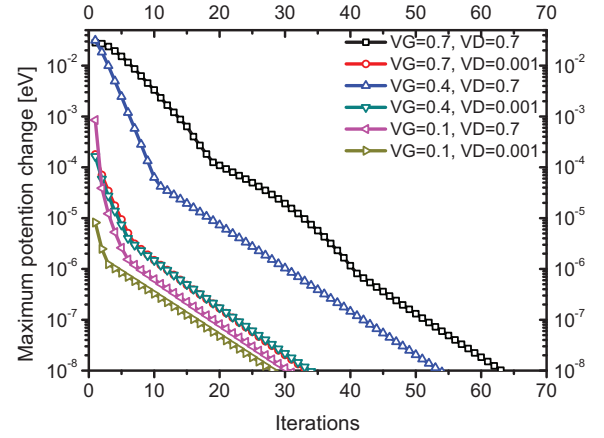


Fig. 3. Convergence behavior of the electrostatic potential for different gate and drain biases.

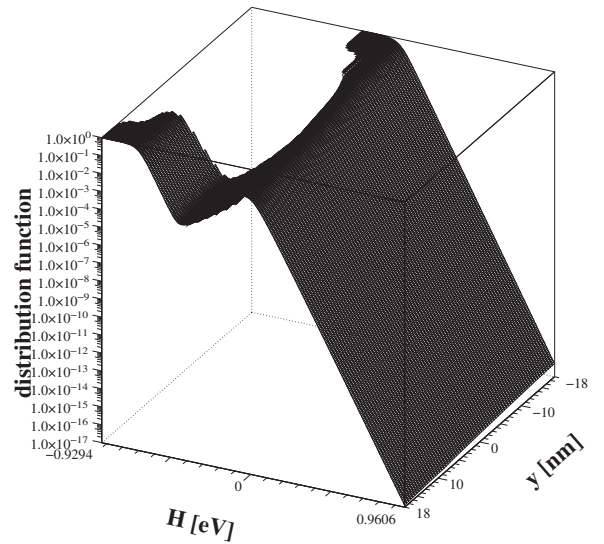


Fig. 4. Electron distribution function of the lowest subband at $V_G=0.7\text{V}$ and $V_D=0.7\text{V}$.

and strong inversion. For all bias conditions the relaxation loop converges in a reliable way.

The lowest order electron distribution functions are shown in Figs. 4, 5 and 6 for the lowest subband. Strong degeneracy, as a consequence of the Pauli principle, can be observed in the lower kinetic energy region. If a large drain bias is applied, the distribution functions near the drain show a large high-energy quasi-ballistic tail. The periodic structures are due to multiple optical phonon scattering. Since scattering is weak, the rightmost local maximum is the highest one.

The input and output characteristics are shown in Fig. 7 and Fig. 8, respectively. Not only the saturation behavior can be simulated, but also the subthreshold region, where the CPU time is actually much lower for subthreshold due to the weaker coupling between the very low channel charge and the electrostatic potential and the better initial guess. Without problems, the current can be calculated over more

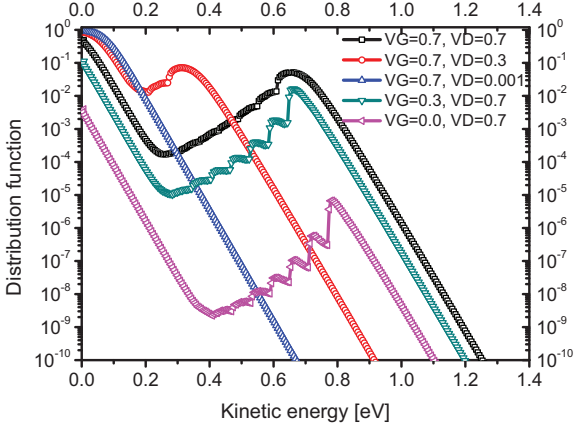


Fig. 5. Electron distribution function of the lowest subband for different gate and drain voltages at position $y=8\text{nm}$.

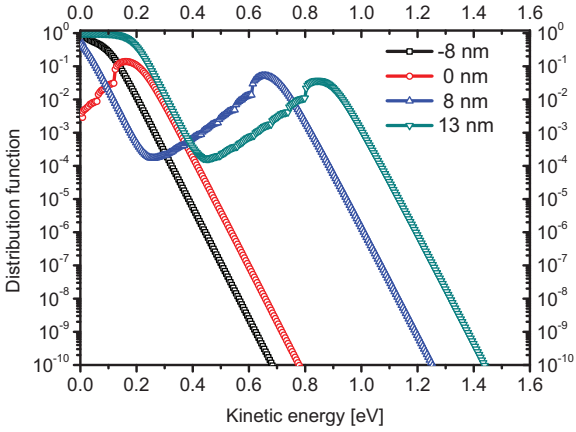


Fig. 6. Electron distribution function of the lowest subband at different slices for $V_G=0.7\text{V}$ and $V_D=0.7\text{V}$

than four orders of magnitude (Fig. 7). The forward and backward currents are shown in Fig. 9. Since transport is quasi-ballistic, the forward current is much larger than the backward. Fig. 10 shows the electron sheet density along the transport direction for different bias conditions. Again, huge variations in the electron density cause no problems. As in the case of the distributions functions the electron density is smooth and no artificial oscillations occur, as they would without proper stabilization.

The cutoff frequency calculated in the quasi-stationary limit [9] is shown in Fig. 11. Due to the high accuracy of the stationary solution, calculation of this small-signal quantity by numerical differentiation is very stable and CPU efficient.

IV. CONCLUSION

A deterministic 2D device simulator for nMOSFETs based on the SE, PE and stationary BTE has been developed, where the H-transformation and the maximum entropy dissipation scheme are introduced in contrast to previous works [3] leading to considerable improvement of stability. The solver yields robust convergence, truly stationary solutions and stable

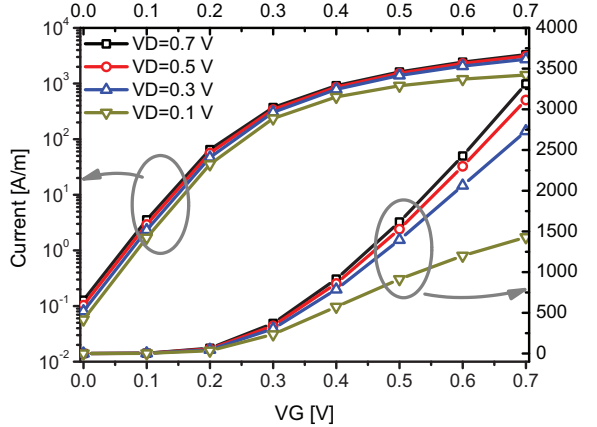


Fig. 7. Input characteristics

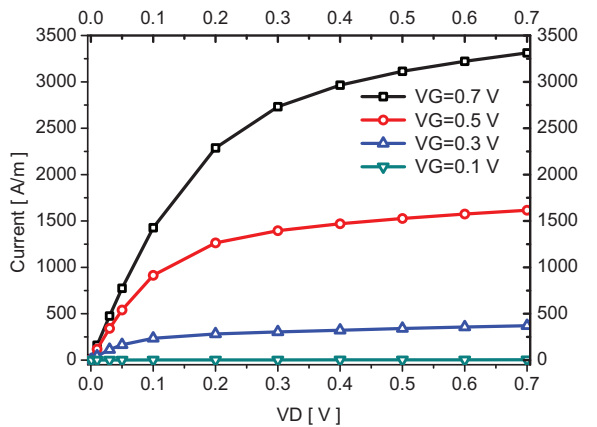


Fig. 8. Output characteristics

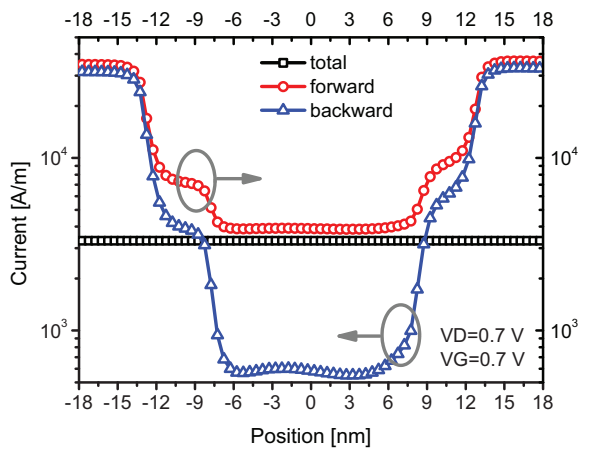


Fig. 9. Electron current at $V_G=0.7\text{V}$ and $V_D=0.7\text{V}$

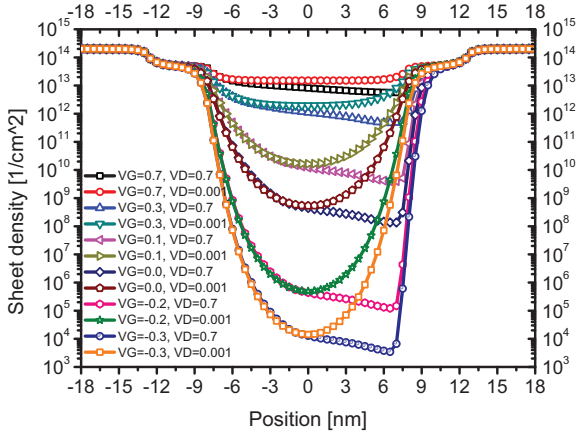


Fig. 10. Electron sheet density

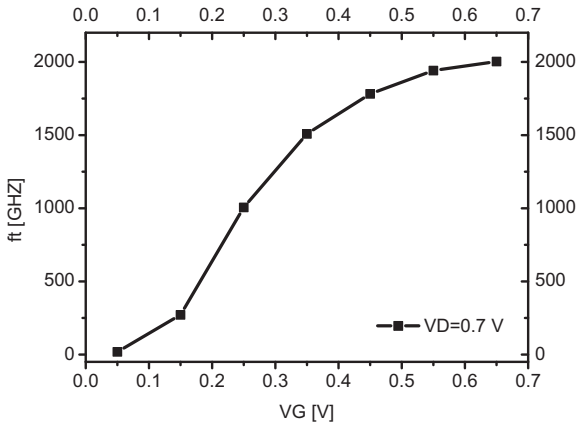


Fig. 11. Cutoff frequency

results even for subthreshold.

ACKNOWLEDGMENT

The first author would like to thank the Deutscher Akademischer Austausch Dienst (DAAD) for their support of this research program.

REFERENCES

- [1] M. V. Fischetti and S. E. Laux, "Monte Carlo study of electron transport in silicon inversion layers," *Phys. Rev. B*, vol. 48, no. 4, pp. 2244–2274, 1993.
- [2] Luca Lucci, Pierpaolo Palestri, David Esseni, Lorenzo Bergagnini, and Luca Selmi, "Multisubband monte carlo study of transport, quantization, and electron-gas degeneration in ultrathin soi n-mosfets," *IEEE Trans. Electron Devices*, vol. 54, no. 5, pp. 1156–1164, 2007.
- [3] A. Pham, C. Jungemann, and B. Meinerzhagen, "On the numerical aspects of deterministic multisubband device simulations for strained double gate pmosfets," *J. Computational Electronics*, vol. 8, no. 3, pp. 242–266, 2009.
- [4] P. Dollfus, D. Querlioz, J. Saint-Martin, V.-N. Do, A. Bournel, "Wigner monte carlo approach to quantum transport in nanodevices," *Proc. SIS-PAD*, pp. 277–280, 2008.
- [5] C. Jungemann, A. Emunds, and W. L. Engl, "Simulation of linear and nonlinear electron transport in homogeneous silicon inversion layers," *Solid-State Electron.*, vol. 36, no. 11, pp. 1529–1540, 1993.
- [6] A. Gnudi, D. Ventura, G. Baccarani, and F. Odeh, "Two-dimensional MOSFET simulation by means of a multidimensional spherical harmonics expansion of the Boltzmann transport equation," *Solid-State Electron.*, vol. 36, no. 4, pp. 575 – 581, 1993.

- [7] C. Ringhofer, "Numerical methods for the semiconductor Boltzmann equation based on spherical harmonics expansions and entropy discretizations," *Transport Theory and Statistical Physics*, vol. 31, no. 4-6, pp. 431–452, 2002.
- [8] S.-M. Hong and C. Jungemann, "A fully coupled scheme for a Boltzmann-Poisson equation solver based on a spherical harmonics expansion," *J. Computational Electronics*, vol. 8, no. 3, pp. 225–241, 2009.
- [9] H. K. Gummel, "On the definition of the Cutoff Frequency f_T ," *Proc. IEEE*, p. 2159, 1969.